Magnetic Resonance Imaging 62 (2019) 209–213

Contents lists available at ScienceDirect

Magnetic Resonance Imaging

journal homepage: www.elsevier.com/locate/mri

Case report

On using signal magnitude in diffusion magnetic resonance measurements of restricted motion

Alpay Özcan

Biomedical Imaging Research and Development Laboratory, and Department of Biomedical Device Technologies, Acıbadem Mehmet Ali Aydınlar University, Kayışdağı, Cad., No:32, 34752, Ataşehir, İstanbul, Turkey

ARTICLE INFO

Keywords:
Magnetic resonance imaging
Diffusion
Diffusion-weighted magnetic resonance imaging
Fourier transform

ABSTRACT

Tissue microstructure has significance as a biomarker, however its accurate inference with diffusion magnetic resonance (MR) is still an open problem. With few exceptions, diffusion weighted (DW) MR models either process diffusion MR data using signal magnitude, whereby microstructural information is forcefully confined to symmetry due to Fourier transform properties, or directly use symmetric basis expansions.

Herein, information loss from magnitude utilization is demonstrated by numerically simulating particles undergoing diffusion near a fully reflective infinite wall and an orthogonal corner.

Simulation results show that the loss of the Hermitian property when using signal magnitude impedes DW–MR from accurately inferring microstructural information in both of the geometries.

1. Introduction

Tissue microstructure, which can be inferred by molecular motion measurements, has high significance as a biomarker. However, accurate inference of restricted motion with diffusion MR is still an open problem. Several models are in use [1], and with few exceptions [2, 3], DW–MR models process diffusion MR data using signal magnitude thereby confining microstructural information to symmetry due to Fourier transform properties.

Symmetry assumptions might be realistic in isotropic environments such as homogeneous liquids. By contrast, in a complex environment, such as biological tissue, the path traveled by the molecules is determined by the heterogeneous microstructure and thereby displacement asymmetry becomes possible. Two existing basis expansion models, the mean apparent propagator (MAP) model [2] and generalized diffusion tensor [3] model, recognize asymmetry and work on the complex valued DW–MR signal. Likewise, the more recently developed complete Fourier direct magnetic resonance imaging (CFD–MRI) [4] methodology treats the complex valued signal and the distribution of the displacement integrals without any symmetry constraints by establishing a high dimensional Fourier relationship between them.

However, direct utilization of symmetric templates in model matching methods such as symmetric tensors of diffusion tensor imaging (DTI) [5, 6] or spherical harmonics of high angular resolution diffusion imaging (HARDI) [7], and/or symmetry by way of signal magnitude in the Fourier based q-space methodologies [8-10] is now standard. This raises the concern that information is being automatically distorted and/or lost by collapsing the asymmetry within the signal, thereby impeding accurate inference. As analytical solutions of DW–MR signal processing exist only for simple geometries such as infinite parallel plates [11, 12], planar, cylindrical and spherical geometries [13], [8]; a proof of principle is needed for emphasizing and revising the importance of concerns regarding loss of information when using symmetry based methods.

Herein, DW–MR inference inaccuracies when using signal magnitude are demonstrated by simulating MR signal from diffusing molecules near an infinite reflective wall and an orthogonal corner. While these two basic geometries are not necessarily representatives of biological tissue's microstructure, they provide solid test beds for analyzing and comparing complex valued data versus magnitude usage in the treatment of diffusion MR signal originating from asymmetric environments.

For properly demonstrating the fundamental concept, the simulations were comprised of pulsed gradient spin echo (PGSE) nuclear magnetic resonance (NMR) experiments without any imaging gradients.

2. Material and methods

2.1. Theory

For modeling coherent or incoherent motion, the time-dependent position of magnetic moments is represented in the most general

E-mail address: alpay.ozcan@acibadem.edu.tr.

https://doi.org/10.1016/j.mri.2019.06.015
Received 4 March 2019; Received in revised form 23 June 2019; Accepted 23 June 2019

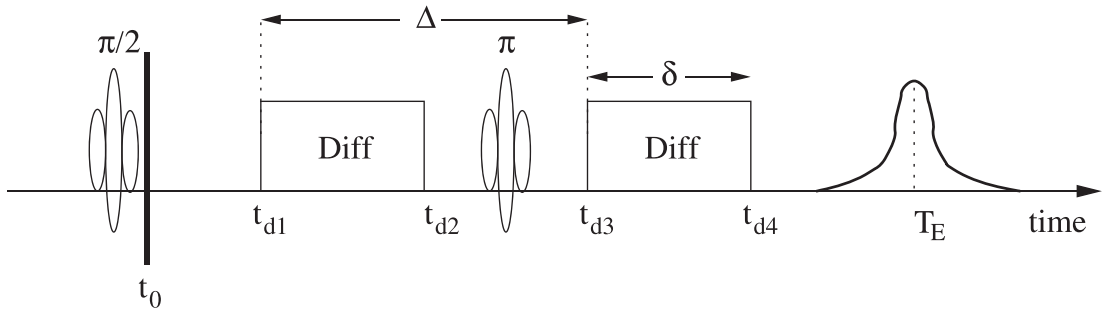

Fig. 1. The PGSE–NMR pulse sequence and the definition of the variables used in the calculations. Sampling starts before the echo time T_E to capture the peak value of the spin echo which is attenuated according to the motion sensitizing magnetic field gradients.

fashion [4]:

$$x_i(t) = x_i(t_0) + w_i(t) \tag{1}$$

using non-interacting particles. In Eq. (1), $w_i(t) \in \mathbb{R}^3$ represents the displacement of the ith magnetic moment from its initial position $x_i(t_0)$ (i.e., $w_i(t_0) = 0$). The initial time t_0 is chosen as the end time of the $\pi/2$ radio frequency (RF) pulse (see Fig. 1). The model covers any type of motion with only the assumption of path continuity since a magnetic moment cannot disappear at a given point and reappear at another.

The NMR signal, on the other hand, is modeled as the sum of the individual transverse magnetization vectors [14], m_i, which is written in complex number form:

$$M(t) = \sum_i m_i(t) = m_0 \sum_i e^{-j\,\gamma\,\Omega_i}. \tag{2}$$

Here, γ is the gyromagnetic ratio and m_0 is the initial magnetization tipped to the transverse plane at the end of the $\pi/2$ RF pulse at t_0 (see Fig. 1). The phase is obtained by multiplying γ and Ω_i, which is ideally a function of the magnetic field gradients and the position of the magnetic moment $x_i \in \mathbb{R}^3$. When ideal rectangular gradient pulses with amplitude vector $G_D \in \mathbb{R}^3$ as in Fig. 1 are applied, Ω_i becomes:

$$\Omega_i = G_D \cdot \left(\int_{t_{d3}}^{t_{d4}} x_i(\tau)\, d\tau - \int_{t_{d1}}^{t_{d2}} x_i(\tau)\, d\tau \right). \tag{3}$$

where t_{d1}, t_{d3} represent on- and t_{d2}, t_{d4} off-times of the pulsed gradients.

Following the derivations in [4] that use the time parameters of Fig. 1, the DW–MR signal model's central theme is the displacement integral. For the PGSE sequence of Fig. 1 the displacement integral of the ith magnetic moment is defined as [4]:

$$W_i^{\mathrm{d}} \doteq \int_{t_{d3}}^{t_{d4}} x_i(\tau)\, d\tau - \int_{t_{d1}}^{t_{d2}} x_i(\tau)\, d\tau = \int_{t_{d3}}^{t_{d4}} w_i(\tau)\, d\tau - \int_{t_{d1}}^{t_{d2}} w_i(\tau)\, d\tau \in \mathbb{R}^3. \tag{4}$$

Additionally, the PGSE parameters δ (pulse length) and Δ (pulse separation) are defined as: $\delta \doteq t_{d2} - t_{d1} = t_{d4} - t_{d3}$ and $\Delta \doteq t_{d3} - t_{d1} = t_{d4} - t_{d2}$ (see also Fig. 1). This is basically the difference of the integrals of the paths traveled by magnetic moments during the pulsed gradients.

According to Eq. (2) and applying Eq. (3) for the pulsed gradients of the PGSE sequence of Fig. 1, the total magnetization at the echo time T_E is a function of the pulsed gradient vector (i.e. the motion sensitizing magnetic field gradient vector), G_D, and the displacement integral W_i^{d}

$$S_{\mathrm{cfd}}^{\mathrm{nmr}} = m_0 \sum_i e^{-j\,\gamma\,G_D \cdot W_i^{\mathrm{d}}}. \tag{5}$$

Rather than computing Eq. (5) over the (finite) count of magnetic moments, a more convenient expression is obtained by defining $P_{\mathrm{cfd}}^{\mathrm{nmr}}(W^{\mathrm{d}})$ as the fraction of magnetic moments with displacement integral value equal to W^{d} (per unit interval, dW^{d}). Using the distribution of displacement integrals, $P_{\mathrm{cfd}}^{\mathrm{nmr}}(W^{\mathrm{d}})$, $S_{\mathrm{cfd}}^{\mathrm{nmr}}$ at the echo time T_E in Fig. 1 is calculated in the (continuous) displacement integral space for obtaining the signal $S_{\mathrm{cfd}}^{\mathrm{nmr}}$:

$$S_{\mathrm{cfd}}^{\mathrm{nmr}} = \int P_{\mathrm{cfd}}^{\mathrm{nmr}}(W^{\mathrm{d}})\, e^{-j\,\gamma\,G_D \cdot W^{\mathrm{d}}}\, dW^{\mathrm{d}}, \tag{6}$$

where both sides of the equation are divided by m_0 for ease of notation. This formulation is general and existing models can in fact be derived starting from Eq. (6) [1, 15].

The expression of Eq. (6) is exactly the Fourier transform of $P_{\mathrm{cfd}}^{\mathrm{nmr}}$ evaluated at the three dimensional frequency vector k_D:

$$S_{\mathrm{cfd}}^{\mathrm{nmr}}(k_D) = \mathcal{F}\{P_{\mathrm{cfd}}^{\mathrm{nmr}}\}(k_D), \tag{7}$$

where $k_D = [k_{D1}, k_{D2}, k_{D3}] = \gamma\, G_D \in \mathbb{R}^3$ represents the pulsed (or diffusion/motion sensitizing) gradient vector with its entries equal to the amplitudes of the pulsed magnetic field gradients of PGSE [4] scaled by γ.

In other words, for each point $k_D \in \mathbb{R}^3$, the Fourier transform of $P_{\mathrm{cfd}}^{\mathrm{nmr}}$ is sampled at the corresponding acquisition. Consequently, $P_{\mathrm{cfd}}^{\mathrm{nmr}}$, which is the physical quantity of interest, is recovered with the inverse Fourier transform of the signal obtained from the MR scanner:

$$P_{\mathrm{cfd}}^{\mathrm{nmr}}(W^{\mathrm{d}}) = \mathcal{F}^{-1}\{S_{\mathrm{cfd}}^{\mathrm{nmr}}\}(W^{\mathrm{d}}). \tag{8}$$

Using the properties of the Fourier transform, Eq. (8) provides crucial information on the nature of $S_{\mathrm{cfd}}^{\mathrm{nmr}}$. The Fourier transform of a real valued function is a **complex valued** Hermitian function [16]. By the reciprocity property of the Fourier transform [16] only symmetric real valued functions' Fourier transforms are real valued. Therefore, $S_{\mathrm{cfd}}^{\mathrm{nmr}}(k_D)$ in Eq. (7) is **complex valued** Hermitian since $P_{\mathrm{cfd}}^{\mathrm{nmr}}(W^{\mathrm{d}})$ is real valued. Furthermore, when there are coherent displacements such as bulk motion, Eq. (4) incorporates a bias term which in turn reflects as a phase shift in $S_{\mathrm{cfd}}^{\mathrm{nmr}}(k_D)$ [4].

By contrast, existing q-space models [8-10] use the magnitude of the signal in practice when evaluating the Fourier transform with the hope of filtering out bulk motion [9, pp.1378]. However, experimental DW–MR signal is not necessarily Hermitian symmetric as various factors including but not limited to susceptibility distort it, whereby the signal magnitude becomes asymmetric. When Fourier transformed, the transform of the asymmetric signal magnitude is a **complex valued** Hermitian function and therefore cannot describe a physically meaningful distribution. The solution offered by the q-space methods is to take the magnitude one more time creating a real symmetric function due to Hermitian symmetry in the complex domain.

In short, by taking the magnitude before and after the Fourier transform, q-space methods constrain the outcome to be real valued and symmetric. This raises the concern that more than what was initially intended (e.g., bulk motion removal) is in fact being eliminated unnecessarily.

As it is impossible to fully analytically describe the distribution functions of the displacement integrals, herein, simulations were used to obtain the functions numerically for showing the detrimental effects of using signal magnitude in the calculations.

2.2. Simulations

Scenarios imitating water protons near reflective walls were constructed with $n_{\text{particles}} = 120{,}000$ particles. With a fixed simulation step size (the standard deviation of the increments), non-interacting particle motion was implemented using a hindered random walk with normally distributed increments ($w_i(t)$ in Eq. (1)) with zero mean. This procedure simulated molecular motion propelled by thermal energy (see [17] for an early simulation example). For modeling hinderance caused by the structure, the displacements were modified when a path crossed a wall. Effectively, the path was readjusted by computing the outcome of the elastic collision(s).

There were 3000 simulation steps executed for each particle. For matching the experimental values of PGSE parameters used in an earlier biological phantom work [18] ($\delta = 15$ ms and $\Delta = 30$ ms), simulation values of the same parameters were chosen as $\delta_{\text{sim}} = 1000$ steps and $\Delta_{\text{sim}} = 2000$ steps with a step time of $t_{\text{step}} = 15 \times 10^{-6}$ s, e.g. $\delta = t_{\text{step}}\,\delta_{\text{sim}}$.

The step size, s, of the random walk was calculated based on the diffusion coefficient of water, $D_{\text{water}} = 2.6 \times 10^{-3}$ mm^2/s:

$$s = \sqrt{6\, D_{\text{water}}\quad t_{\text{step}}} = 0.48\ \mu\text{m}. \tag{9}$$

Numerical simulations consisted of: DW–MR Simulations

1. At the initial time step, $k = 0$, uniformly distributing initial positions of the particles near the walls,
2. Calculating the position of the ith magnetic moment in discrete time propelled by thermal energy:
$$x_i(k+1) = x_i(k) + s\ \eta(k), \tag{10}$$
where $\eta(\cdot) \in \mathbb{R}^3$ is (pseudorandom) normally distributed.
3. If the line through $(x_i(k+1), x_i(k))$ crosses a wall, i.e. when hitting a wall, correcting the path by elastic collision computations,
4. Evaluating numerically the displacement integral differences of Eq. (4) using the displacements, $w_i(k)$:
$$W_i^{\text{d}} = t_{\text{step}}\ \left(\left(\sum_{k=K_3}^{K_4} w_i(k)\right) - \left(\sum_{k=K_1}^{K_2} w_i(k)\right)\right) \tag{11}$$
where $t_{\text{step}}\quad \times [K_1\ K_2\ K_3\ K_4] = [t_{d1}\ t_{d2}\ t_{d3}\ t_{d4}]$.
5. Repeating Step 2 through Step 4 for all of the magnetic moments and
6. Computing the distribution, $P_{\text{cfd}}{}^{\text{nmr}}$, of the displacement integral values.

In-house Matlab®, (ver. 2014b, Mathworks, Natick, MA USA) programs were used for all of the computations and visualization. Distributions with 128 bins were calculated using hist and hist3 functions for one and two dimensional simulations respectively. For implementing discrete Fourier transform (DFT) Matlab®'s fast Fourier transform (FFT) routines were used.

3. Results and discussion

Although there are solutions in simple microstructures with planar, spherical and cylindrical geometries [8, 11-13], a full description of information loss from signal magnitude usage in a general geometry is difficult to obtain due to the lack of analytical characterizations of the distribution functions. Herein, Brownian motion near reflecting walls in one and two dimensions, similar to the work in [19, 20], was simulated with the algorithm of Section 2.2 for numerically calculating the distributions.

For one dimensional scenario, a wall was placed on the origin and particles were initially uniformly distributed in an interval starting from the origin ending at 5 different positions: (0 6 μm], (0 13 μm], (0 20 μm], (0 27 μm], (0 34 μm] (see Fig. 2). Simulations were executed and $P_{\text{cfd}}{}^{\text{nmr}}(W^{\text{d}})$ was obtained from the numerically calculated W_i^{d}, $i = 1,\ldots,n_{\text{particles}}$.

Fig. 2 compares distribution functions obtained from different initial conditions. Initial condition intervals extending farther from the wall resulted in more symmetric and spread $P_{\text{cfd}}{}^{\text{nmr}}$, resembling more isotropic motion. In contrast, $P_{\text{cfd}}{}^{\text{nmr}}$'s *asymmetry* is more prominent when particles start near the wall.

For all of the distributions, $\mathcal{F}\{P_{\text{cfd}}^{\text{nmr}}\ \}$ was calculated for simulating DW–MR signal coming out of the MR scanner. As all of the distributions were **asymmetric**, their Fourier transforms were **complex valued Hermitian**. Therefore, the magnitude, $|\mathcal{F}\{P_{\text{cfd}}^{\text{nmr}}\ \}|$, was a real valued symmetric function. As the (inverse) Fourier transform of a real symmetric function is also real symmetric [16], $\mathcal{F}^{-1}\{|\mathcal{F}\{P_{\text{cfd}}^{\text{nmr}}\ \}|\}$ was real and symmetric. This is demonstrated on the right of Fig. 2 by showing the mismatch between $P_{\text{cfd}}{}^{\text{nmr}}$ (asymmetric) and $\mathcal{F}^{-1}\{|\mathcal{F}\{P_{\text{cfd}}^{\text{nmr}}\ \}|\}$ (symmetric).

In the one dimensional scenario which did not incorporate any bulk motion, using signal magnitude, which was claimed to be filtering out bulk motion [9, pp.1378], should have left the distribution intact. Fig. 2 shows that distribution asymmetry is lost and the symmetric distribution obtained from signal magnitude implies wrongly an isotropic medium. In reality, for particles near an elastic wall the motion is anisotropic as reported by the asymmetry of the original distribution.

In two dimensions, two scenarios were run using a vertical wall and a corner, both reflective and placed at the origin (see Fig. 3). For the vertical wall, the initial positions were uniformly distributed on the (0, 20μm] × (0, 5.76 mm] strip (5.76 mm = 0.1 ×s × $n_{\text{particles}}$) and for the corner, the initial distribution was uniform on the square: (0, 20μm] × (0, 20μm] (Fig. 3, left panel).

In Fig. 3's middle panel, accurate inference of the wall geometry was attained as original distributions were analyzed. By contrast, on the right panel, the Fourier transformed magnitude produces symmetric distributions with the appearance of a tube (top) and a box (bottom) rather than a vertical wall and a corner respectively.

Also, taking the magnitude transfers the imaginary portion to the real axis, thereby adding a positive constant to the signal which in turn becomes a spike at [0, 0] in Fig. 3 and at 0 in Fig. 2 when calculating the Fourier transform. This, in turn, inaccurately indicates a large number of magnetic moments with zero displacement integral values, which might mislead inference of mathematical models that include terms for stationary magnetic moments, e.g., of water trapped in small compartments [21, 22], likewise the positive constant term in models using cumulant expansion [23].

4. Conclusions

Biological interpretation of DW–MR information is the subject of active research with new developments using existing model attributes, such as the decrease in the apparent diffusion coefficient caused by neurite beading after ischemic stroke [24] and cerebral cortical gray matter development [25]. New theories describing novel attributes are also being developed for the same purpose, e.g., the MAP model [2] where the focus is the microstructure in brain tissue.

The purpose of the DW–MR, like any other imaging modality, is the inference of biological properties with the aim of producing informative biomarkers. This is accomplished in two steps starting from the MR scanner's output signal that is Fourier transformed for reconstructing the physically meaningful displacement integral distribution:

$$S_{\text{cfd}}\quad \rightarrow P_{\text{cfd}}\quad \rightarrow \text{Biological properties}$$

In the process, intermediate steps must be carried out carefully while respecting physically meaningful information content.

This work demonstrated that, as shown in Fig. 2 and Fig. 3, the usage of magnitude may result in incorrect information:

$$\mathcal{F}^{-1}\{|S_{\text{cfd}}^{\text{nmr}}\ |\} \neq P_{\text{cfd}}^{\text{nmr}}\quad = \mathcal{F}^{-1}\{S_{\text{cfd}}^{\text{nmr}}\ \}, \tag{12}$$

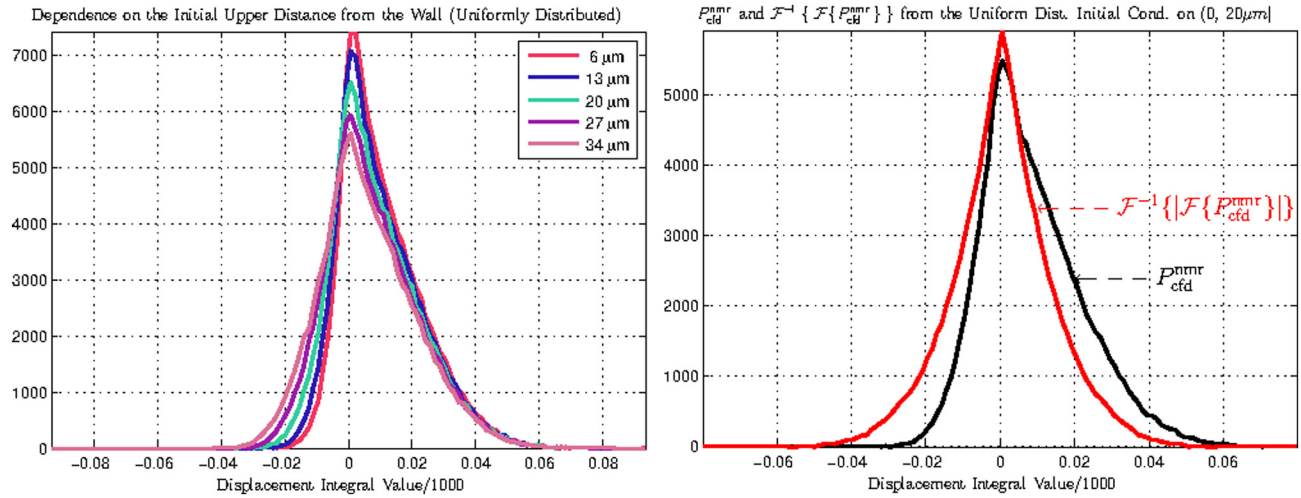

Fig. 2. On the left, the displacement integral distributions corresponding to one dimensional simulations with a reflective wall placed at the origin. The legend indicates color coding of the curves depending on the upper limit of the initial condition interval. As the upper limit increases, i.e. more particles start far away from the wall, $P_{cfd}{}^{nmr}$ becomes more symmetric and spread, appearing more like isotropic motion. On the right, the mismatch between the original *asymmetric* distribution (black) and the Fourier inversion of the magnitude (red) of the distribution's Fourier transform, $\mathcal{F}^{-1}\{|\mathcal{F}\{P_{cfd}^{nmr}\}|\}$, is shown for the initial condition interval (0 20 μm]. Note the larger number of zero displacement integrals that are inaccurately inferred using the distribution (red) obtained with signal magnitude. (For interpretation of the references to color in this figure legend, the reader is referred to the web version of this article.)

potentially hampering accurate inference of microstructure.

The proof was achieved in an ideal simulated environment with minimal assumptions, e.g. without including loss of magnetization at the walls [26, 27], wall permeability [28] and particle interactions. While no mathematical model is perfect, falsification when validating under ideal conditions is a legitimate reason for abandoning a model or at least using prudence in interpreting the model's outcomes. For future in and ex vivo diffusion imaging research, rather than assuming that diffusion profiles in biological tissue are symmetric for any reason, it would be prudent to adopt DW–MR models incorporating asymmetry

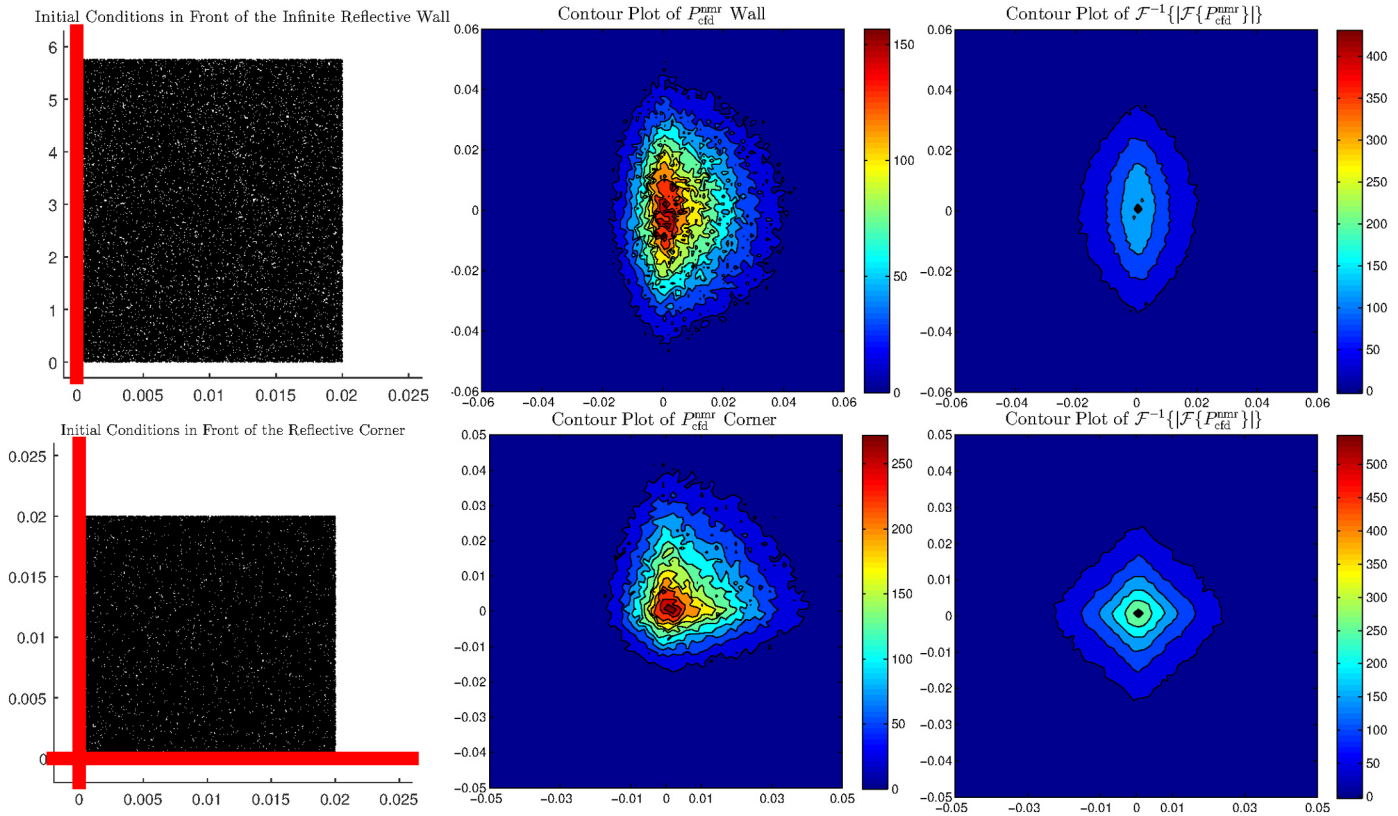

Fig. 3. On the left, initial uniform particle placement for the infinite reflective wall (top) and the corner (bottom) scenarios. The contour plots of the displacement integral distributions are shown in the middle panel demonstrating accurately the trend of particles bouncing from the wall(s). On the top, the distribution is skewed to the right implying the presence of the wall. On the bottom, spread beam shaped distribution indicates the presence of a corner. On the right column, using signal magnitude creates inaccurate distributions. The wall is inferred as a vertically oriented tube (top) and the corner appears as a box (bottom). Furthermore, there is a large spike at the origin of both distributions inaccurately indicating a large number of particles with zero displacement integrals.

assumptions and let the data analysis indicate symmetry and/or lack thereof.

Accordingly, instead of using signal magnitude, the solution offered by CFD–MR [4] is based on re-establishing Hermitian symmetry of the complex valued signal collected from the MR scanner by using systemic phase correction algorithms. For example, bulk motion appears as a linear phase which is rigorously handled with a linear phase correction algorithm in the Fourier domain [4]. However, factors which are beyond the scope of this manuscript, including but not limited to susceptibility effects, distort the Hermitian symmetry of the DW–MR signal in a nonlinear fashion. Development of algorithms for analyzing and subsequently correcting those effects remains an open question for future research. Furthermore, using complex valued signal in CFD–MR automatically removes nonlinear Rician restrictions [29] on noise modeling in DW–MR.

In conclusion, this paper mainly concentrated on the first step that constitutes the foundation for biological property inference, namely removing signal magnitude processing from DW–MR methods with the aim of improving accurate reconstruction of physical quantities. Simulations in fundamental geometries demonstrated that the usage of signal magnitude in diffusion MR can significantly distort the estimation of motion describing distributions, and hence may impede accurate inference of microstructure.

Acknowledgments

This work was supported by the Scientific and Technological Research Council of Turkey's (TÜBİTAK) 3001 funding program, titled "Simulating Microstructure Inferred from Diffusion Magnetic Resonance Imaging and Modelling Effects of the MR Scanner on the Diffusion MR Signal", grant number 118E304.

The author would also like to extend his special thanks to John Gore and the reviewers for their valuable insights and progressive feedback.

References

[1] Özcan A, Wong KH, Larson-Prior L, Cho Z-H, Mun SK. Background and mathematical analysis of diffusion MRI methods. International Journal of Imaging Systems and Technology 2012;22(1):44–52. https://doi.org/10.1002/ima.22001: https://doi.org/10.1002/ima.22001.

[2] Özarslan E, Koay CG, Shepherd TM, Komlosh ME, İrfanog-lu MO, Pierpaoli C, Basser PJ. Mean apparent propagator (MAP) MRI: a novel diffusion imaging method for mapping tissue microstructure. NeuroImage 2013;78:16–32. https://doi.org/10.1016/j.neuroimage.2013.04.016: http://www.sciencedirect.com/science/article/pii/S1053811913003431.

[3] Liu C, Bammer R, Acar B, Moseley ME. Characterizing non-gaussian diffusion by using generalized diffusion tensors. Magnetic Resonance in Medicine 2004;51(5):924–37.

[4] Özcan A. Complete fourier direct magnetic resonance imaging (CFD–MRI) for diffusion MRI. Frontiers in Integrative Neuroscience 2013;7(18). https://doi.org/10.3389/fnint.2013.00018: http://www.frontiersin.org/integrative_neuroscience/10.3389/fnint.2013.00018/abstract.

[5] Basser P, Mattiello J, Lebihan D. Estimation of the effective self-diffusion tensor from the NMR spin echo. Journal of Magnetic Resonance, Series B 1994;103(3):247–54. https://doi.org/10.1006/jmrb.1994.1037: http://www.sciencedirect.com/science/article/pii/S1064186684710375.

[6] Mattiello J, Basser P, Lebihan D. Analytical expressions for the b matrix in NMR diffusion imaging and spectroscopy. Journal of Magnetic Resonance, Series A 1994;108(2):131–41. https://doi.org/10.1006/jmra.1994.1103: http://www.sciencedirect.com/science/article/pii/S106418588471103X.

[7] Frank LR. Anisotropy in high angular resolution diffusion-weighted MRI. Magnetic Resonance in Medicine 2001;45(6):935–1141.

[8] Callaghan, P. T., Dynamics, Translational Resonance, Magnetic, Principles of Pulsed Gradient Spin Echo NMR, Oxford University Press Oxford England, New York, 2011.

[9] Wedeen VJ, Hagmann P, Tseng W-YI, Reese TG, Weisskoff RM. Mapping complex tissue architecture with diffusion spectrum magnetic resonance imaging. Magnetic Resonance in Medicine 2005;54(6):1377–85.

[10] Tuch DS. Q–ball imaging. Magnetic resonance in medicine 2004;52(6):1358–72.

[11] Wayne RC, Cotts RM. Nuclear-magnetic-resonance study of self-diffusion in a bounded medium. Phys. Rev 1966;151:264–72. https://doi.org/10.1103/PhysRev.151.264: https://link.aps.org/doi/10.1103/PhysRev.151.264.

[12] Robertson B. Spin-echo decay of spins diffusing in a bounded region. Phys. Rev 1966;151:273–7. https://doi.org/10.1103/PhysRev.151.273: https://link.aps.org/doi/10.1103/PhysRev.151.273.

[13] Barzykin A. Theory of spin echo in restricted geometries under a step-wise gradient pulse sequence. Journal of Magnetic Resonance 1999;139(2):342–53. https://doi.org/10.1006/jmre.1999.1778. URL: http://www.sciencedirect.com/science/article/pii/S1090780799917780.

[14] Brown R, Cheng Y, Haacke E, Thompson M, Venkatesan R. Magnetic Resonance Imaging: Physical Principles and Sequence Design. New York: John Wiley and Sons; 2014.

[15] Özcan A. Comparison of the complete Fourier direct MRI with existing diffusion weighted MRI methods. Proceedings of the 2011 IEEE International Symposium on Biomedical Imaging. Chicago, Illinois USA; 2011. p. 931–4.

[16] Bracewell RN. The Fourier Transform and Its Applications, 3rd Edition, McGraw-Hill Series in Electrical and Computer Engineering, Circuits and Systems, McGraw Hill ill.; 25 cm. Includes bibliographical references and index. Boston: (DLC) 99021139 Ronald N. Bracewell; 2000.

[17] Ermak DL. A computer simulation of charged particles in solution. I. Technique and equilibrium properties. The Journal of Chemical Physics 1975;62(10):4189–96. https://doi.org/10.1063/1.430300: https://doi.org/10.1063/1.430300.

[18] Özcan A, Quirk J, Wang Y, Wang Q, Sun P, Spees W, Song S-K. The validation of complete fourier direct MR method for diffusion MRI via biological and numerical phantoms. Engineering in Medicine and Biology Society,EMBC, 2011 Annual International Conference of the IEEE 2011:3756–9. https://doi.org/10.1109/IEMBS.2011.6090640.

[19] Özarslan E, Koay CG, Basser PJ. Remarks on q-space MR propagator in partially restricted, axially-symmetric, and isotropic environments. Magnetic Resonance Imaging 2009;27(6):834–44. https://doi.org/10.1016/j.mri.2009.01.005: http://www.sciencedirect.com/science/article/pii/S0730725X09000113.

[20] Özarslan E, Nevo U, Basser PJ. Anisotropy induced by macroscopic boundaries: surface-normal mapping using diffusion-weighted imaging. Biophysical Journal 2008;94(7):2809–18. https://doi.org/10.1529/biophysj.107.124081: http://www.sciencedirect.com/science/article/pii/S0006349508705320.

[21] Alexander DC, Hubbard PL, Hall MG, Moore EA, Ptito M, Parker GJ, Dyrby TB. Orientationally invariant indices of axon diameter and density from diffusion MRI. NeuroImage 2010;52(4):1374–89. https://doi.org/10.1016/j.neuroimage.2010.05.043: http://www.sciencedirect.com/science/article/pii/S1053811910007755.

[22] Panagiotaki E, Schneider T, Siow B, Hall MG, Lythgoe MF, Alexander DC. Compartment models of the diffusion MR signal in brain white matter: a taxonomy and comparison. NeuroImage 2012;59(3):2241–54. https://doi.org/10.1016/j.neuroimage.2011.09.081: http://www.sciencedirect.com/science/article/pii/S1053811911011566.

[23] Kroenke CD, Bretthorst GL, Inder TE, Neil JJ. Modeling water diffusion anisotropy within fixed newborn primate brain using bayesian probability theory. Magnetic Resonance in Medicine 2006;55(1):187–97.

[24] Budde MD, Frank JA. Neurite beading is sufficient to decrease the apparent diffusion coefficient after ischemic stroke. Proceedings of the National Academy of Sciences 2010;107(32):14472–7. https://doi.org/10.1073/pnas.1004841107: http://www.pnas.org/content/107/32/14472.abstract.

[25] Kroenke CD. Using diffusion anisotropy to study cerebral cortical gray matter development. Journal of Magnetic Resonance 2018;292:106–16. https://doi.org/10.1016/j.jmr.2018.04.011: http://www.sciencedirect.com/science/article/pii/S1090780718301150.

[26] Snaar J, Vanas H. NMR self-diffusion measurements in a bounded system with loss of magnetization at the walls. Journal of Magnetic Resonance, Series A 1993;102(3):318–26. https://doi.org/10.1006/jmra.1993.1110: http://www.sciencedirect.com/science/article/pii/S1064185883711101.

[27] Sen PN, Schwartz LM, Mitra PP, Halperin BI. Surface relaxation and the long-time diffusion coefficient in porous media: periodic geometries. Phys. Rev. B 1994;49:215–25. https://doi.org/10.1103/PhysRevB.49.215: https://link.aps.org/doi/10.1103/PhysRevB.49.215.

[28] Tanner JE. Transient diffusion in a system partitioned by permeable barriers. Application to NMR measurements with a pulsed field gradient. The Journal of Chemical Physics 1978;69(4):1748–54. https://doi.org/10.1063/1.436751: https://doi.org/10.1063/1.436751.

[29] Gudbjartsson H, Patz S. The Rician distribution of noisy MRI data. Magnetic Resonance in Medicine 1995;34(6):910–4.